

Laser-induced dissociative ionization of H_2 from the near-IR to the mid-IR regime

Qingli Jing and Lars Bojer Madsen

Department of Physics and Astronomy, Aarhus University, 8000 Aarhus C, Denmark

(Dated: October 18, 2018)

We apply the Monte Carlo Wave Packet (MCWP) approach to investigate the kinetic energy release (KER) spectra of the protons following double ionization in H_2 when interacting with laser pulses with central wavelengths ranging from the near-IR (800 nm) to the mid-IR (6400 nm) regions and with durations of 3-21 laser cycles. We uncover the physical origins of the peaks in the nuclear KER spectra and ascribe them to mechanisms such as ionization following a resonant dipole transition, charge-resonance-enhanced ionization (CREI) and ionization in the dissociative limit of large internuclear distances. For relatively large pulse durations, i.e., for 15 or more laser cycles at 3200 nm and 10 or more at 6400 nm, it is possible for the nuclear wave packet in H_2^+ to reach very large separations. Ionization of this part of the wave packet results in peaks in the KER spectra with very low energies. These peaks give direct information about the dissociative energy in the $2p\sigma_u$ potential energy curve of H_2^+ at the one- and three-photon resonances between the $2p\sigma_u$ and $1s\sigma_g$ curves in H_2^+ . With the MCWP approach, we perform a trajectory analysis of the contributions to the KER peaks and identify the dominant ionization pathways. Finally, we consider a pump-probe scheme by applying two delayed pulses to track the nuclear dynamics in a time-resolved setting. Low-energy peaks appear for large delays and these are used to obtain the $2p\sigma_u$ dissociative energy values at the one-photon resonance between the $2p\sigma_u$ and $1s\sigma_g$ curves in H_2^+ for different wavelengths.

PACS numbers: 33.20.Xx, 33.40.+f, 33.80.Eh,

I. INTRODUCTION

The significant advances in femtosecond laser technology have opened the possibility to control chemical reactions with laser light [1–3]. When exposing molecules to intense laser pulses, strong interaction between molecules and the external electromagnetic field may give rise to electronic excitation or even result in ionization. Nuclear dynamics is hence often induced because of the interplay between the nuclei and electrons. A good example is the process of dissociative ionization [4, 5], a process in which dissociation is induced as a result of the removal of one or more electrons. Laser-induced dissociative ionization has received considerable interests in the past two decades [6–8]. Thanks to the fast developments in imaging techniques such as COLTRIMS [9] and VMI spectrometers [10], it is now possible to measure the kinetic energy of the ionic fragments or the liberated electrons or both. By analysing the kinetic energy release (KER) spectra of the ionic fragments, information about the ionization process can be obtained [11]. For example, both the process of charge-resonance-enhanced-ionization (CREI) [12, 13] and resonance-enhanced multiphoton ionization [14, 15] manifest themselves through the occurrence of characteristic peaks in the nuclear KER spectra [16]. Different from the mechanism of resonance-enhanced multiphoton ionization, for one-electron system like H_2^+ , CREI results from lowering the internal barrier between the double wells at certain critical internuclear separations in the presence of a strong field, along with the creation of a pair of field-dressed charge-resonant states.

In parallel to the advances in experimental techniques, many theoretical methods [17–19] have been developed and proven to work very well in describing a range of phenomena associated with the interaction of molecules

and light. Among these methods, the Monte Carlo wave packet (MCWP) approach [20, 21] performs well when describing the laser-induced dissipative dynamics. Especially in previous works on H_2 [22, 23], and O_2 [24], where the nuclear KER spectra were of main concern, the simulations agreed very well with the measurements. This approach, like many others, is devoted to solve the time-dependent Schrödinger equation, but the problem is greatly simplified as the electronic degrees of freedom are treated in an effective description. At the same time, the Markov approximation [25] is applied, which means that the flow of electrons from the molecular systems to the surroundings is uni-directional and irreversible. The loss of electrons is encoded in jump operators, which are responsible for jumps among different Hilbert spaces and constitute a non-Hermitian part of the total Hamiltonian. The non-Hermitian Hamiltonian implies that the norm of the system is decreasing over time. The drop of the norm over time is controlled by the instantaneous ionization rates [26, 27] of the system. If the ionization rates depend on the nuclear configuration, wave packet motion is induced in the neutral molecule. Inducing nuclear dynamics in this way is called Lochfraß [28–30] and this phenomena is an integrated part of the MCWP simulations. In the present MCWP approach to dissociative ionization, the jumps between different charge states and associated Hilbert spaces are described by ionization rates. While the evolution of the system within a given charge state is coherent, the rate treatment of the ionization step means that coherence between the remaining cation and the ionized electron is lost. Also we have no knowledge of the energy distribution of the outgoing electron.

Recently there has been a shift in strong-field physics towards the use of mid-IR driving wavelengths [31], e.g.,

to image molecular structures by light-induced electron diffraction (LIED) [32, 33] and to greatly increase the photon energies of high-harmonic generation (HHG) [34]. The interaction between the mid-IR laser pulses and molecules can be treated in the quasi-static regime. To our knowledge, the behavior of the nuclear KER spectra with increasing wavelength from the near-IR region to the mid-IR region has not been studied systematically. Such a systematic investigation of the trends in the spectra and the underlying physics when going to longer wavelengths is the topic of the present work. The large wavelengths of the intense IR laser pulses make the ionization dynamics of molecules enter the regime of tunneling ionization [35–38]. Studying the peaks in the KER spectra at mid-IR wavelengths can help to obtain detailed knowledge of the nuclear motion, as will be discussed below. As a characteristic trend in the spectra, we see a shift towards lower KER values with increasing wavelength.

The paper is organized as follows. In Sec. II, we review how to apply the MCWP method to simulate dissociative ionization in H_2 . In Sec. III, we discuss the KER spectra obtained for H_2 exposed to laser pulses with different wavelengths and pulse durations. In Sec. IV, the nuclear KER spectra of H_2 interacting with pump-probe pulses with delays are analyzed. Sec. V concludes. Atomic units ($\hbar = e = m_e = a_0 = 1$) are used throughout unless stated otherwise.

II. MCWP APPROACH FOR DISSOCIATIVE IONIZATION OF H_2

The MCWP approach for dissociative ionization was described in detail elsewhere [21–24, 40], so the description here is brief. The dissipative dynamics of a diatomic molecule interacting with laser light can be described by the time-dependent Schrödinger equation (TDSE)

$$i\partial_t|\Psi(t)\rangle = H(t)|\Psi(t)\rangle = (H_s - \frac{i}{2} \sum_m C_m^\dagger C_m)|\Psi(t)\rangle, \quad (1)$$

with the Hermitian Hamiltonian

$$H_s = T_N + V_N + V_{eN} + T_e + V_{ee} + V_I(t), \quad (2)$$

where T_N is the kinetic energy operator for the nuclei, T_e the kinetic energy for the electrons, V_N the nuclear repulsion, V_{eN} the nuclei-electron interaction, V_{ee} the electron-electron interaction and $V_I(t)$ the laser-matter interaction. Within the Born-Oppenheimer approximation, the total state $|\Psi(t)\rangle$ can be expanded as

$$|\Psi(t)\rangle = \sum_m \int d\vec{R} X_m(\vec{R}, t) |\phi_{R,m}^{el}\rangle \otimes |\vec{R}\rangle, \quad (3)$$

in which $X_m(\vec{R}, t)$ is the nuclear wave packet and $|\vec{R}\rangle$ refers to the position eigenkets of the nuclear coordinate. The electronic basis states $|\phi_{R,m}^{el}\rangle$ can be obtained by

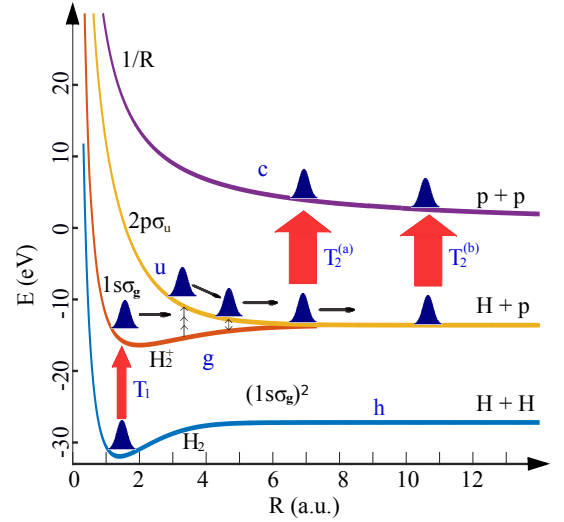


FIG. 1. Sketch of four field-free Born-Oppenheimer electronic potential energy curves [39]. These curves are the $(1s\sigma_g)^2$ ground-state curve in H_2 labeled by h , the $1s\sigma_g$ and $2p\sigma_u$ curves in H_2^+ labeled by g and u , respectively, and the $1/R$ Coulombic curve labeled by c . A particular realization of a quantum trajectory with the MCWP approach is also shown: At some instant T_1 , the first ionization occurs and the neutral wave packet is promoted to the singly-ionized system where coherent evolution takes place. At some later instant T_2^j ($j = a, b$), the second ionization occurs and then the nuclei undergo Coulomb repulsion. The final energy of the protons depends on the instants T_1, T_2^j .

solving the time-independent Schrödinger equation with parametric dependence on the internuclear separation \vec{R} :

$$(T_e + V_{ee} + V_{eN} + V_N)|\phi_{R,i}^{el}\rangle = E_{el,i}(R)|\phi_{R,i}^{el}\rangle, \quad (4)$$

where $E_{el,i}(R)$ is the corresponding electronic potential energy curve. The four electronic potential energy curves included in our MCWP calculations are shown in Fig. 1. These are the $(1s\sigma_g)^2$ curve in H_2 , the $1s\sigma_g$ and $2p\sigma_u$ curves in H_2^+ , and the doubly-ionized Coulombic curve in H_2^{++} - for short denoted h, g, u , and c , respectively. These curves were previously shown to be sufficient to capture the dynamics responsible for the KER spectra [22, 23]. The jump operators C_m in Eq. (1) constitute a non-Hermitian term in the total Hamiltonian. This term is responsible for the jumps among the different Hilbert spaces of H_2, H_2^+ and H_2^{++} ,

$$C_m = \int d\vec{R} \sqrt{\Gamma_m(\vec{R}, t)} |\phi_{R,n}^{el}\rangle \langle \phi_{R,m}^{el}| \otimes |\vec{R}\rangle \langle \vec{R}|, \quad (5)$$

where $\Gamma_m(\vec{R}, t)$ is the ionization rate from the m (h, g or u) state to the n (g, u or c) state and depends on the instantaneous value of the field strength. In this work, the ionization rate responsible for the ionization of H_2 is calculated using the weak-field asymptotic theory of Ref. [37]. The ionization rates for the ionization of the

cation are obtained by interpolating the results published in Ref. [41].

By substituting Eqs. (3), (4) and (5) into Eq. (1) and using the ansatz $X_m(\vec{R}, t) = \frac{1}{R} K_m(R, t) W_m(\theta, \phi, t)$, the time evolution of the radial wave function $K_m(R, t)$ can be obtained. As the molecule is assumed rotationally frozen during the interaction with the femtosecond laser pulse, the angular parts of the nuclear wave function $W_m(\theta, \phi, t)$ can be expressed as $W_m(\theta, \phi, t) = \frac{1}{\sqrt{4\pi}} \delta(\theta - \theta_0) \delta(\phi - \phi_0)$ with θ_0 and ϕ_0 specifying the internuclear orientation. In the calculations below, we consider the case where the molecule is aligned with the linear polarization of the external field, i.e., $\theta_0 = 0^\circ$ and $\phi_0 = 0^\circ$, where the latter can be arbitrary because of symmetry.

The simulation procedure of the MCWP technique is outlined in the following (see also Refs. [22, 23]). The nuclear wave function first evolves in the neutral system with its norm square decreasing because of the non-Hermitian term in the Hamiltonian. At each time step, the drop in the norm square is compared with a random number (between 0 and 1), which determines whether the jump from one Hilbert space to another takes place or not. If the drop in the norm square is larger than the random number, ionization occurs and thus the wave function jumps, is renormalized and then evolves in the new Hilbert space, otherwise, ionization can not occur and the wave function needs to be renormalized in the neutral system. The comparison between the drop in the norm square and a random number continues until the first jump occurs. Similarly, whether the second jump takes place or not is controlled by comparing the drop in the norm square of the nuclear wave function in H_2^+ with a new random number (between 0 and 1). The difference compared to the first jump is that there are two pathways for the second jump to the doubly-ionized system, from the g state curve and from the u state curve, which means that another random number (between 0 and 1) should be introduced to decide which pathway to choose. As a result, a nuclear wave function after emitting two electrons is obtained stochastically, with the first jump occurring at some instant of time T_1 and the second jump at some instant of later time T_2 [Fig. 1]. The nuclear wave packet after two jumps $K_c(R, T_2)$ holds all the information of the nuclei. For example, the nuclear kinetic energies can be obtained through projecting the wave packet on Coulomb waves $K_E(R)$,

$$\text{KER}_m(T_1, T_2) = \left| \int K_E(R) K_c(R, T_2) dR \right|^2, \quad (6)$$

with $m = g, u$. Equation (6) only gives the KER signal for one stochastic event occurring at specific T_1 and T_2 . We refer to such a specific realization of jump times and dynamics as a quantum trajectory. The total nuclear KER spectra of the dissociative ionization process can be obtained by averaging over all the stochastic events. In the present case of dissociative double ionization, the

computational effort can, however, be dramatically reduced through eliminating all the random numbers by applying a completely deterministic approach. To this end, the two jumps which are dressed with probabilities are assumed to take place at every time step. Actually, the probability for each jump is proportional to the drop in the norm square at that jump time. This is reasonable as the larger the drop in the norm square, the more likely it is for a jump to occur. Summing over all the weighted events, the nuclear KER spectra can be obtained from the formula,

$$\text{KER}_{\text{tot}} = \sum_{T_1, T_2} P_1 P_{12} \sum_{m=g, u} P(m|\{T_1, T_2\}) \text{KER}_m(T_1, T_2). \quad (7)$$

In the above equation, $P_1 = -d(N_h(t))/dt$ is the probability density for the first jump with $N_h(t)$ representing the norm square of the nuclear wave function of the h state; $P_{12} = -d(N_g(t) + N_u(t))/dt$ is the conditional probability density of the second jump for a given first jump with $N_g(t)$ and $N_u(t)$ representing the norm square of the nuclear wave function of the g state and the u state, respectively; and $P(m|\{T_1, T_2\}) = \langle \Psi | C_m^+ C_m | \Psi \rangle / \langle \Psi | C_g^+ C_g + C_u^+ C_u | \Psi \rangle$ is the conditional probability density from the m (g or u) state for given first and second jump times (see also Ref. [40]).

As shown in Fig. 1, the initial nuclear wave function is assumed to be ground state of the $(1s\sigma_g)^2$ potential energy curve of H_2 . The applied laser pulse with polarization axis parallel to the molecular axis first kicks out the first electron and then induces nuclear motion in the two potential energy curves of the H_2^+ system. Meanwhile, there is electronic dipole coupling between the $1s\sigma_g$ and $2p\sigma_u$ states. Finally, the nuclei experience Coulomb repulsion after emitting the second electron. Thus the nuclei pick up energy from two terms, one is the dissociative kinetic energy in the singly-ionized system and the other is the Coulomb repulsion energy in the doubly-ionized system. The time-dependent Hamiltonian, including the non-Hermitian part representing the interaction between states in different Hilbert spaces as well as the electronic dipole coupling between states within a given Hilbert space, originates from the external laser field. As a result and as shown in the next section, the kinetic energy is closely related to the parameters of the applied laser pulse, such as peak intensity, wavelength, and pulse duration.

Numerically, within each Hilbert space, we solve the TDSE by applying the split-operator method [42] on the short-time propagator, i.e.,

$$U(t + \Delta t, t) = \exp(-iT_N \frac{\Delta t}{2}) \exp(-iV(R, t + \frac{\Delta t}{2}) \Delta t) \times \exp(-iT_N \frac{\Delta t}{2}). \quad (8)$$

Obviously, it is the term $V(R, t)$ that determines how the wave packet evolves in each Hilbert space. For example, in H_2^+ , the 2-by-2 matrix representation of $V(R, t)$

is $V_{ij}(R, t) = E_{el,i}(R)\delta_{ij} - i\Gamma_i(R, t)\delta_{ij} + \beta D_{ij}(R)F(t)$ ($i, j = g, u$), where $\beta = 1 + 1/(2m_p + 1)$ with m_p the proton mass, $F(t)$ is the electric field, and $D_{ij}(R)$ is the electronic dipole moment function between i and j states along the direction, $\hat{\epsilon}$, of the linear polarization, i.e., $D_{ij}(R) = -\langle \phi_{R,i}^{el} | \vec{r} \cdot \hat{\epsilon} | \phi_{R,j}^{el} \rangle$. We use the explicit expression for $D_{gu}(R) = \frac{R}{2\sqrt{1 - ((1+R+R^2/3)e^{-R})^2}} - \frac{1}{(2+1.4R)}$ given in Ref. [43]. The size of our simulation box is 40.96. The time step Δt is 0.1 and the spatial step ΔR is 0.02. The operators $\exp(-iT_N \frac{\Delta t}{2})$ and $\exp(-iV(R, t + \frac{\Delta t}{2})\Delta t)$ are diagonal in the momentum and position representations, respectively, thus a fast-Fourier-transform algorithm is applied in the implementation.

III. WAVELENGTH AND PULSE DURATION DEPENDENCE OF KER SPECTRA FOR H_2 INTERACTING WITH A SINGLE LASER PULSE

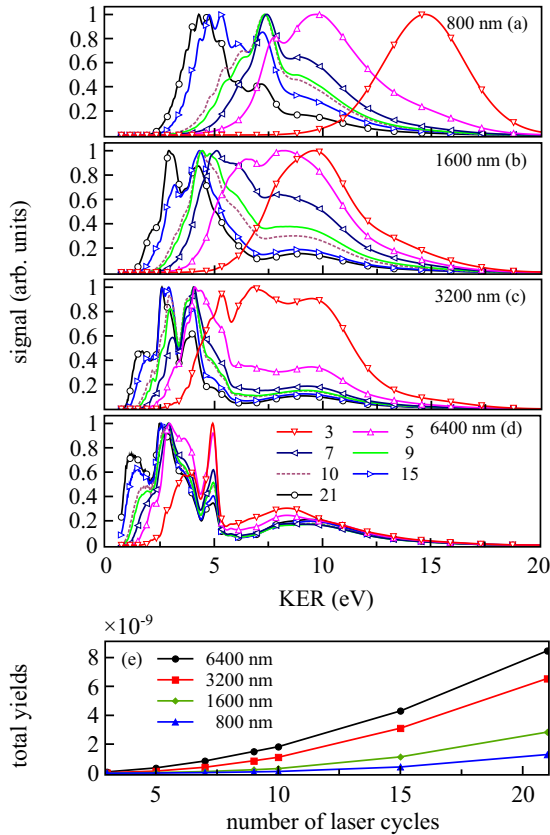


FIG. 2. (a)-(d) Renormalized nuclear KER spectra after double ionization of H_2 interacting with laser pulses with different wavelengths ranging from 800 nm to 6400 nm and with different FWHM pulse durations ranging from 3 to 21 laser cycles. All the pulses have a peak intensity of $6 \times 10^{13} \text{ W/cm}^2$. (e) Total yields of protons in units of ionization probability per molecule as a function of the number of laser cycles for several wavelengths.

In this section, we simulate the process of dissociative

double ionization of ground-state H_2 interacting with single laser pulses. The calculated proton KER spectra for different wavelengths (ranging from 800 nm to 6400 nm) and pulse durations (ranging from 3 to 21 laser cycles) are shown in Fig. 2. In our calculation, the laser pulses are of Gaussian shape, and the pulse durations are expressed in terms of the number of laser cycles within the FWHM of the intensity profile of the applied laser pulses. The laser intensity of $6 \times 10^{13} \text{ W/cm}^2$ is chosen to be similar to the one in the experiment of Ref. [44]. If there are specific internuclear positions from which a significant part of the second ionization takes place, distinctive peaks occur in the nuclear KER spectra. These peaks mostly come from events in H_2^+ which occur at internuclear separations with a resonant one- or three-photon dipole coupling between the $1s\sigma_g$ and $2p\sigma_u$ curves, or at the separations of CREI [12, 13], or in the dissociative limit beyond the CREI distances. When we look at Fig. 2 from the top to the bottom, we see in general that the KER spectra move towards lower kinetic energies with increasing duration of the laser pulses. This behavior is because the larger the duration of the pulse, the more likely it is for the nuclei to dissociate to larger separations with correspondingly smaller repulsive Coulomb energy. Moreover, when interacting with laser pulses with the same duration, for example 10 laser cycles at 800 nm and 5 laser cycles at 1600 nm, even though the individual peaks are shifted because of the different positions for the resonant electronic dipole coupling in H_2^+ , the overall widths of the KER spectra windows look quite similar. We will now identify the most prominent peaks in the spectra in Fig. 2. The special KER peak around 9 eV visible in Figs. 2(a-d), is a signature of the outer turning point of the nuclear wave packet evolving along the $1s\sigma_g$ BO potential energy curve in H_2^+ . The peak is nearly independent of the laser pulse and is in nice agreement with the classical estimate of the Coulomb repulsion energy of $1/R_{tp} \sim 1/3$ (9.1 eV), with $R_{tp} \sim 3$ the outer turning point of the wave packet along the $1s\sigma_g$ potential energy curve, when the initial nuclear wave packet is assumed to be that of the ground state of the $(1s\sigma_g)^2$ curve with an equilibrium internuclear separation of 1.4.

For a fixed wavelength, several peaks in the KER spectra are more or less at similar positions for different numbers of laser cycles within the FWHM intensity duration. This behavior is a signature of the fact that the positions of the resonant electronic one- and three-photon dipole coupling are the same for these laser pulses. Moreover, there are clear signatures of CREI [13] in the spectra. CREI takes place at internuclear separations around $R = 7$ and $R = 11$ [41] at this laser peak intensity, and gives rise to Coulomb repulsive energies of 3.9 eV and 2.5 eV. When the wavelength is larger, the distances between positions for the one- or three-photon resonance and positions for CREI are smaller, and thus the dissociative kinetic energy picked up along the $2p\sigma_u$ curve before the CREI positions is becoming smaller. The peaks around 3 eV (smaller than the Coulomb repulsion at $R = 7$) in

Figs. 2(b-d) is a signature of CREI around $R = 11$, while in Fig. 2(a) the pulse durations are too short to allow a substantial portion of the nuclear wave packet to reach $R = 11$ during the pulse.

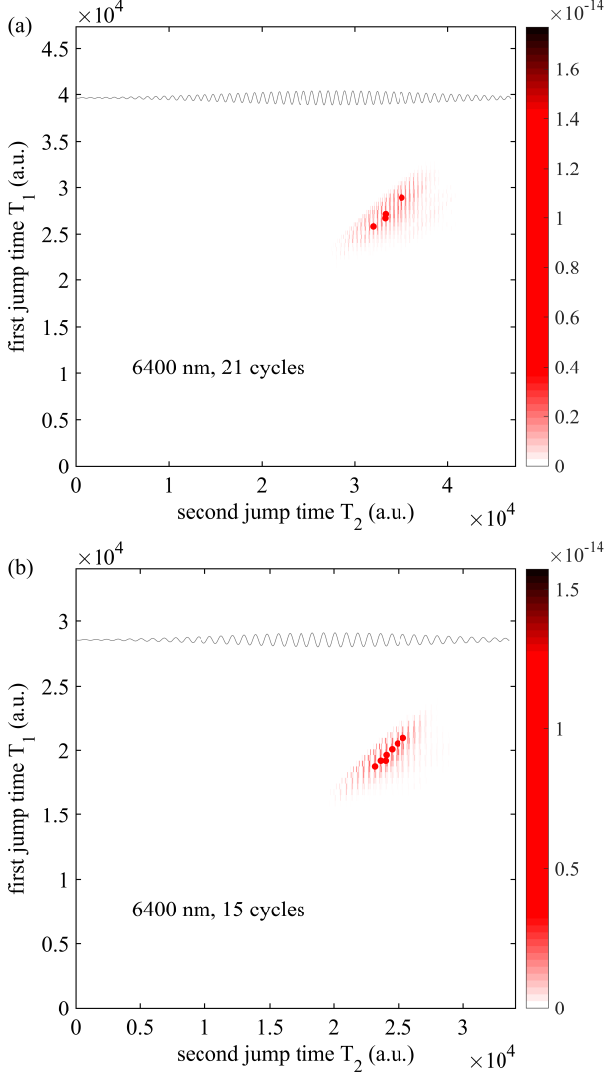


FIG. 3. (a) Contributions from different trajectories to the low-energy peak around 1.2 eV in Fig. 2(d) when interacting with a pulse with 21 laser cycles at 6400 nm. (b) Contributions from different trajectories to the low-energy peak around 1.5 eV in Fig. 2(d) when interacting with a pulse with 15 laser cycles at 6400 nm. The red dots in (a) and (b) mark the trajectories which give the largest contributions. The laser pulses are indicated by the grey lines and the parameters are as in Fig. 2(d).

When interacting with laser pulses with larger wavelengths, see Figs. 2(c) and 2(d), some pronounced new energy peaks appear around 1.5 eV when the number of laser cycles is larger than 15 (10) for 3200 nm (6400 nm). These peaks occur because the nuclear wave packet can move further during the longer pulse and be ionized at separations beyond the positions of CREI. These

low-energy peaks are of the same origin as the < 2 eV peak monitored in a previous pump-probe experiment [45]. The low-energy peaks for 15 and 21 laser cycles at 6400 nm are at about 1.5 eV and 1.2 eV, respectively. We benefit from the stochastic sampling within the MCWP approach and carry out a trajectory analysis of these two peaks. The contributions from different trajectories are shown in Fig. 3. The ionization rate from the $2p\sigma_u$ state to the doubly-ionized molecule is at least one order of magnitude larger than that from the $1s\sigma_g$ state for $R \geq 3$ [41]. Moreover, only a very small part of the nuclear wave packet reaches distances $R > 3$ via evolution on the $1s\sigma_g$ curve. Thus the nuclear wave packet evolving along the $2p\sigma_u$ curve contributes much more to the low-energy KER peaks. As a result, only trajectories where the second jump takes place from the $2p\sigma_u$ state are shown in Fig. 3. A clear oscillatory dependence of the signal on the second jump time T_2 can be observed. This is because all the first jumps take place at the field extrema and there are enhancements when the second jumps occur near field extrema. The time differences between the second and first jumps are the evolution times within the H_2^+ system. The evolution times for the most prominent events (marked by red dots) for 21 and 15 laser cycles are about 6190 (150 fs) and 4420 (108 fs), which correspond to 7 and 5 laser cycles, respectively. In this manner, the MCWP approach allows us to find the typical time spent in the H_2^+ system, i.e., the time needed to ionize H_2^+ , for each particular feature in the KER spectra. These times are long enough for the nuclear wave packets to reach quite large internuclear separations ($R > 20$) along the dissociative $2p\sigma_u$ potential energy curve. As we will now show the difference (2 laser cycles for the two peaks at 1.2 eV and 1.5 eV in Fig. 2(d)) between the two evolution times allows us to obtain the dissociative kinetic energy E_d for the low-energy peaks.

One can see from Fig. 1 that there is nearly no variation in the $2p\sigma_u$ potential energy curve when $R > 8$. Thus the dissociative kinetic energies of the low-energy protons are almost the same in spite of different numbers of laser cycles and ionization from different internuclear separations larger than 8. We can therefore estimate the dissociation energies in the following way. We consider two equations $E_d + 1/R_{21} = 1.2$ eV and $E_d + 1/R_{15} = 1.5$ eV, with R_{21} and R_{15} denoting the positions where the second ionization takes place when interacting with laser pulses with 21 and 15 laser cycles, respectively. In combination with the use of the relations $E_d = \frac{1}{2}mv^2$ and $vt = R_{21} - R_{15}$, we obtain the dissociative kinetic energies along the $2p\sigma_u$ potential energy curve from both the positions of the one- and three-photon resonances between the $2p\sigma_u$ and $1s\sigma_g$ curves. In these equations, v is the velocity corresponding to E_d , m here is the reduced mass of the nuclei, and t is the evolution time difference for the 1.5 eV and 1.2 eV peaks. By substituting the evolution time difference of 2 laser cycles into the above equations, two physical solutions of the dissociative kinetic energy are obtained. One is 0.12 eV corresponding to the disso-

TABLE I. Data used for the analysis of the nuclear KER spectra following dissociative double ionization of H_2 . The 750 nm case will be considered in Sec. IV. Here ω denotes the laser angular frequency. R_1 and R_3 are the positions of the one- and three-photon resonances between the $2p\sigma_u$ and $1s\sigma_g$ curves in H_2^+ , respectively. E_{u1} and E_{u3} are the corresponding potential energies in the $2p\sigma_u$ potential energy curve at R_1 and R_3 . a_0 is the Bohr radius.

$\lambda(\text{nm})$	$\hbar\omega(\text{eV})$	$R_1(a_0)$	$R_3(a_0)$	$E_{u1}(\text{eV})$	$E_{u3}(\text{eV})$	$1/R_1(\text{eV})$	$1/R_3(\text{eV})$
800	1.55	4.74	3.28	-12.69	-10.7	5.7	8.3
1600	0.775	5.64	4.22	-13.14	-12.23	4.8	6.4
3200	0.388	6.5	5.12	-13.35	-12.91	4.2	5.3
6400	0.194	7.32	6	-13.46	-13.24	3.7	4.5
750	1.653	4.67	3.19	-12.63	-10.47	5.82	8.53

ciative kinetic energy via the one-photon resonance. The other is 0.47 eV which corresponds to the dissociative kinetic energy after the three-photon resonance. Thus the potential energies at the one- and three-photon resonances can be expected as $-13.6 \text{ eV} + 0.12 \text{ eV} = -13.48 \text{ eV}$ and $-13.6 \text{ eV} + 0.47 \text{ eV} = -13.13 \text{ eV}$, where -13.6 eV is the energy of the dissociation limit. Both the energies obtained are quite close to the energies in the $2p\sigma_u$ curve of -13.46 eV and -13.24 eV at the one- and three-photon resonances as listed in Table I. In a similar way, we can obtain the potential energies of the $2p\sigma_u$ curve at the one- and three-photon resonances between the $2p\sigma_u$ and $1s\sigma_g$ curves for 3200 nm.

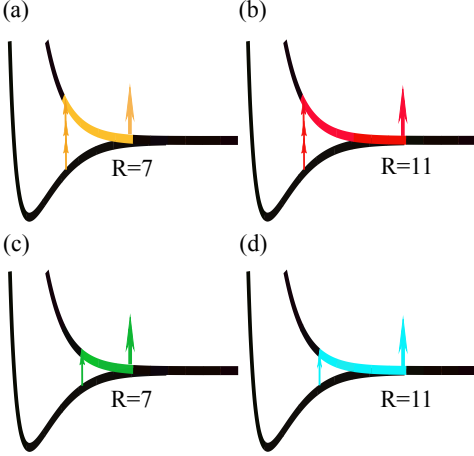


FIG. 4. Sketch of four processes of enhanced ionization at the two CREI positions of $R = 7$ and $R = 11$ (denoted by the outermost right arrows in the figures) after one- and three-photon resonance transitions. (a) and (b) CREI at $R = 7$ and $R = 11$ after the three-photon resonance. (c) and (d) CREI at $R = 7$ and $R = 11$ after the one-photon resonance.

A detailed analysis of the KER spectra in Fig. 2 is conducted in the following with reference to Table I. The four processes shown in Fig. 4 are expected to play an important role for the final nuclear KER spectra. They are representing enhanced ionization at the two CREI positions after the one- and three-photon resonant dipole

coupling between the $1s\sigma_g$ and the $2p\sigma_u$ states in H_2^+ at smaller internuclear distances. In principle, ionization at the one- and three-photon resonances should also result in peaks close to their Coulomb repulsion energies as the dissociative kinetic energy is much smaller for these two cases. To better understand the origin of the peaks in Fig. 2, the positions of the one-photon resonance, R_1 , and the three-photon resonance, R_3 , are given in Table I for several wavelengths. In addition, the potential energies in the $2p\sigma_u$ potential energy curve (E_{u1} and E_{u3}) and in the Coulomb potential energy curve for H_2^{++} at R_1 and R_3 are given.

When the wavelength is 800 nm, as expected from Table I, there should be some enhancement in the proton yields at around 8.3 eV, 5.7 eV, 6.6 eV, 5.36 eV, 4.63 eV and 3.4 eV. They result from enhanced ionization at the three-photon resonance and the one-photon resonance as well as from the four processes pictured in Fig. 4. In Fig. 2(a), the peaks around 4.7 eV mainly come from enhanced ionization at the CREI position of $R = 7$ via the one-photon resonance, which can be verified by the following process: The dissociative kinetic energy is $13.43 \text{ eV} - 12.69 \text{ eV} = 0.74 \text{ eV}$, which is the difference in the $2p\sigma_u$ potential energy curve between $R_3 = 3.28$ and $R = 7$. Adding this kinetic energy to the Coulomb repulsion energy $1/7$ (3.89 eV) at $R = 7$, the total kinetic energy of the proton is 4.63 eV. Similarly, the peaks around 5.3 eV in Fig. 2(a) can be related to enhanced ionization at the CREI position of $R = 11$ via the three-photon resonance, which are quite close to the expected $2.89 \text{ eV} + 2.47 \text{ eV} = 5.36 \text{ eV}$. The peaks around 7.3 eV are indeed from the combined contributions from at least two processes. These are enhanced ionization at the three-photon resonance (8.3 eV) and at the CREI position of $R = 7$ via the three-photon resonance (6.6 eV). These two relative broad peaks may give a peak at around $(8.3 \text{ eV} + 6.6 \text{ eV}) / 2 = 7.45 \text{ eV}$. The peaks around 6.2 eV are mainly from the combination of enhanced ionization at the one-photon resonance (5.7 eV) and at the CREI position of $R = 7$ via the three-photon resonance (6.6 eV).

When the wavelength is 1600 nm, Table I and reasoning as in the 800 nm case above shows that enhancements around 6.4 eV, 4.8 eV, 4.2 eV, 3.0 eV, 5.1 eV and 3.9 eV are expected to appear in the spectra shown in Fig. 2(b). As a result, the peaks around 6.4 eV mainly come from enhanced ionization via the three-photon resonance. The peaks around 5 eV are mainly from enhanced ionization at $R = 7$ after the three-photon resonance. The peaks around 4.3 eV are mainly from enhanced ionization at the CREI position of $R = 7$ and enhanced ionization at $R = 11$ via the three-photon resonance. Besides, large ionization at the CREI position of $R = 11$ through the one-photon resonance leads to the peaks around 3 eV.

As the wavelength increases to 3200 nm, the expected enhancements in the spectra are around 5.3 eV, 4.2 eV, 4.0 eV, 2.8 eV, 4.4 eV and 3.2 eV, respectively [Table I].

The ionization at the three-photon resonance can result in peaks around 5.3 eV. The peaks around 4.0 eV mainly come from large ionization at the one-photon resonance or at the CREI position of $R = 7$ via the one-photon resonance or even from enhanced ionization at $R = 7$ after the three-photon resonance. The peaks around 2.6 eV come from large ionization at the CREI position of $R = 11$ after the one-photon resonance, while the peaks around 3 eV are from enhanced ionization at $R = 11$ after the three-photon resonance. Further increasing the wavelength to 6400 nm, there should be enhancement in the proton yields around five kinetic energies (4.5 eV, 3.7 eV, 2.6 eV, 4.1 eV and 2.9 eV [Table I]). There would be no events at $R = 7$ after the one-photon resonance, as the position of the one-photon resonance $R = 7.32$ is larger than $R = 7$. The one-photon resonance and three-photon resonance give peaks around 3.6 eV and 4.9 eV. Enhanced ionization at the CREI position of $R = 11$ from the one- and three-photon resonances give the respective peaks around 2.6 eV and 2.9 eV.

All of the plots in Figs. 2(a-d) are renormalized to better observe the common features in the spectra. There are large differences in the proton yields for the pulses. In Fig. 2(e), the total yields of protons as a function of the number of laser cycles under several wavelengths are shown in units of ionization probability per molecule, which are also the units for the nuclear KER spectra below. When the peak intensity of the laser pulse is fixed, the duration of the pulse does influence the total yields. The larger the duration, the larger the yield. Besides, for the same durations, e.g., 10 laser cycles at 1600 nm and 5 laser cycles at 3200, the yields are nearly identical.

IV. DELAY DEPENDENCE OF KER SPECTRA FOR H_2 INTERACTING WITH TWO PULSES

When molecules interact with two or more laser pulses, dynamics of the nuclei as well as dynamics of the photoelectrons can be studied as a function of the time delay between the pulses. Usually, the first pulse is the pump which stimulates electronic excitation and nuclear motion. The following pulse acts as the probe and is used to detect the nuclear or electronic wave packets. The pump-probe technique has been widely used to study ultrafast dynamics of both electrons and nuclei and we refer the readers to Refs. [11, 29, 44, 46–48] for recent examples in H_2 . In Fig. 5(a), we plot the simulated KER distributions as a function of time delay between pump and probe laser pulses with their polarization axes parallel to the molecular axis. In order to test the performance of our approach, the parameters of the two laser pulses are chosen according to Ref. [48]: The central wavelength and the FWHM duration of the two pulses are 750 nm and 3 laser cycles, respectively. The pump laser has a peak intensity of 4×10^{14} W/cm² while the probe has a peak intensity of 6×10^{13} W/cm². We find a good agreement between Fig. 5(a) and the experimental results of

Ref. [48]. In particular, the high-energy branch around 10 eV and the energy-decreasing branch from 6 eV to 2 eV for increasing time delay are reproduced.

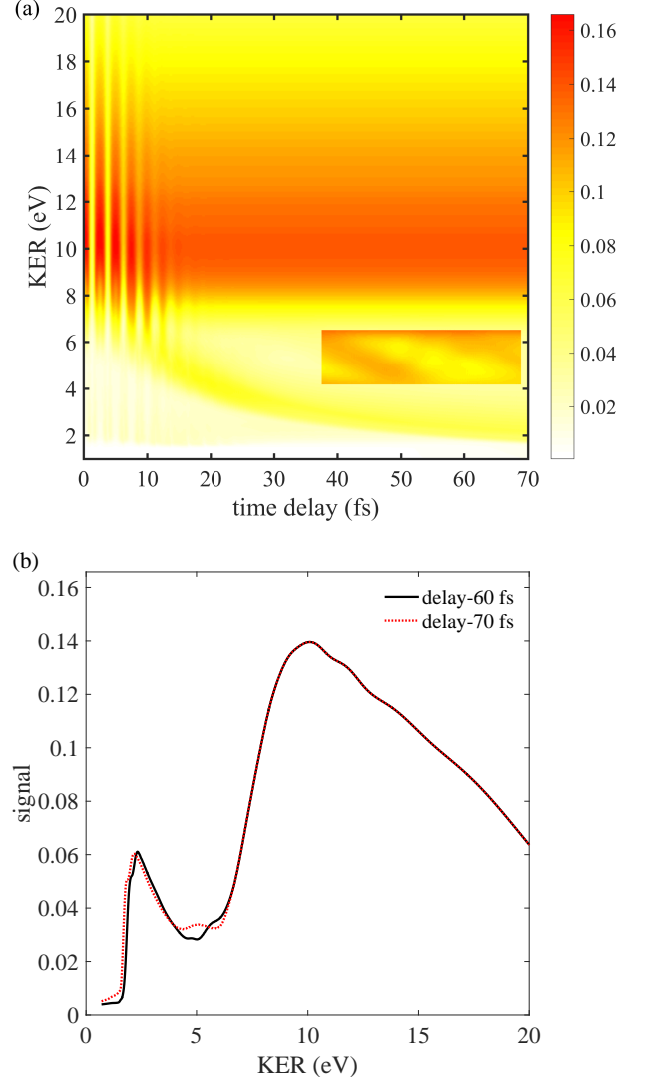


FIG. 5. (a) Nuclear KER distributions as a function of time delay between pump and probe pulses. The peak intensity of the pump (probe) pulse is 4×10^{14} W/cm² (6×10^{13} W/cm²). The two pulses have the same wavelength (750 nm) and the same duration (3 laser cycles). The data are plotted to the power of 0.2 in order to gain a larger visibility of the structures and after that the signal in the insert was multiplied by a factor of 3. (b) Cuts from (a) before multiplying by a factor 3 at time delays of 60 fs and 70 fs.

In Fig. 5(a), the channel with KER around 10 eV mainly comes from double ionization of H_2 by the more intense pump pulse. This channel shows no delay dependence when the delay is larger than 20 fs. However, for delays smaller than 20 fs, oscillation of the KER distributions with a period of one laser cycle is observed. This oscillation is a signature of constructive and destructive interference between the two pulses when the two pulses

overlap in time. The channel with KER in the 2-6 eV range has a strong delay dependence and is due to the ionization of H_2^+ by the relatively weak probe pulse. The main energy-decreasing branch from 6 eV to 2 eV for increasing delay is a result of the nuclear wave packet moving along the $2p\sigma_u$ potential energy curve in H_2^+ . In addition, there are two much weaker energy-decreasing branches. A zoom of part of the branches is shown in the insert to the right of Fig. 5(a). These branches can be shown to result from the oscillatory movement of the nuclear wave packet along the $1s\sigma_g$ potential energy curve in H_2^+ : The duration between the first dominant decreasing branch starting at a time delay around 15 fs and the second branch highlighted in the insert is around 20-25 fs corresponding to a full oscillatory motion in the $1s\sigma_g$ curve. In order to extract properties of the $2p\sigma_u$ potential energy curve, we resort to solving the equations of the dissociative kinetic energy as discussed in Sec. III. We use the peak positions of 2.17 eV and 2.34 eV for the two low-energy peaks at time delays of 60 fs and 70 fs [Fig. 5(b)]. With this difference in evolution time of 10 fs, we obtain the dissociative kinetic energy of about 0.93 eV. Thus the $2p\sigma_u$ potential energy at the one-photon resonance position for 750 nm is about $-13.6 \text{ eV} + 0.93 \text{ eV} = -12.67 \text{ eV}$, which is very close to the expectation of -12.63 eV from Table. I.

As the wavelength of the laser pulses becomes larger, more structures in the KER spectra are expected as the larger laser duration can activate more ionization pathways. In Fig. 6(a), we plot the KER distributions as a function as delay, when the wavelengths of both pulses are 1600 nm while the other parameters are as in Fig. 5. Processes similar to the ones in Fig. 5(a) can be seen in Fig. 6(a). For example, interference between the two pulses at time delays shorter than 30 fs and movement of the nuclear wave packet along the $2p\sigma_u$ potential energy curve (branch decreasing from 5 eV). Three peaks around 10 eV are observed. The origin of these peaks is discussed below. As shown in Fig. 6(b), when the delay is 140 fs, the low-energy peak of the KER spectra is around 1.2 eV, and when the delay is 80 fs, the low-energy peak of the KER spectra is around 1.75 eV. By solving similar equations as in Sec. III, we obtain a dissociative kinetic energy of 0.42 eV, which is used to obtain the potential energy along the $2p\sigma_u$ curve at the one-photon resonance position for 1600 nm. The result of $-13.6 \text{ eV} + 0.42 \text{ eV} = -13.18 \text{ eV}$ is in very good agreement with the energy of -13.14 eV from Table. I.

A trajectory analysis can help to clearly identify how the peaks in Fig. 6(b) are formed. In Fig. 7, contributions from different trajectories to the four peaks (8.5 eV, 9.8 eV, 13 eV and 1.4 eV) in the KER spectra when the delay is 122 fs in Fig. 6(b) are shown. As in Fig. 3, a periodical dependence of the signal with the second jump time T_2 is clearly seen. The three peaks around 8.5 eV, 9.8 eV and 13 eV are mainly from double ionization induced by the pump pulse alone: The signals around 13 eV mainly come from trajectories in which

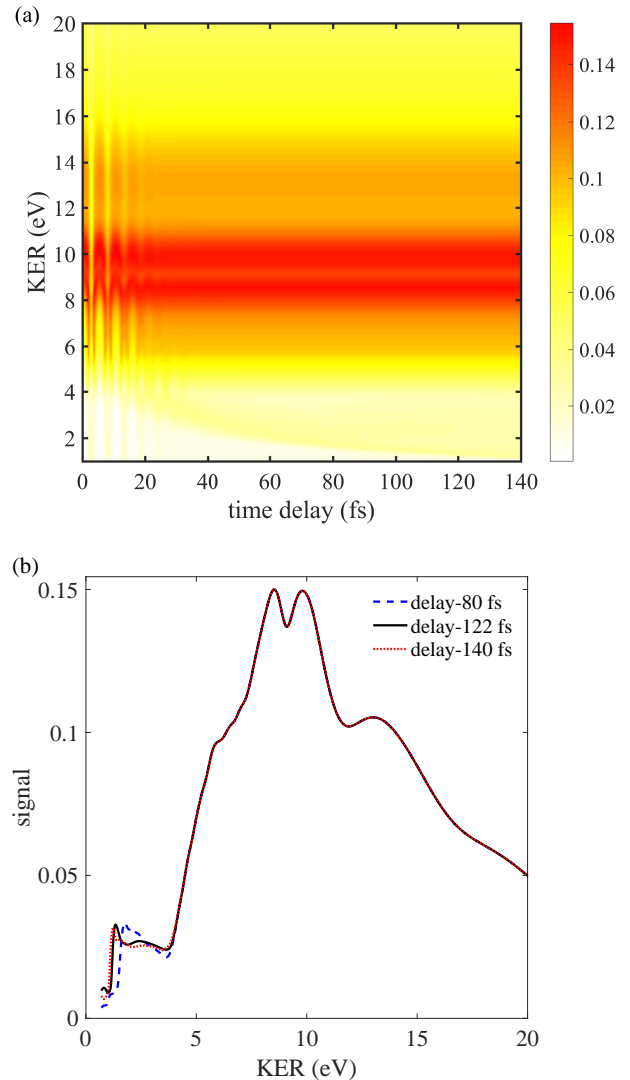


FIG. 6. (a) Nuclear KER distributions as a function of time delay between pump and probe pulses. The peak intensity of the pump (probe) pulse is $4 \times 10^{14} \text{ W/cm}^2$ ($6 \times 10^{13} \text{ W/cm}^2$). Both the wavelengths are 1600 nm and the duration of both pulses is 3 laser cycles. The data are plotted to the power of 0.2 in order to gain a larger visibility of the structures. (b) Cuts from (a) at time delays of 80 fs, 122 fs and 140 fs.

the evolution time in H_2^+ (difference between the first and second jump times) is about half a laser cycle; the signals around 9.8 eV are from trajectories where the evolution time is around one laser cycle; and the signals around 8.5 eV are from trajectories where the evolution time is about one and a half laser cycles. The low-energy peak around 1.4 eV is from trajectories where the first ionization is induced by the pump pulse and the second by the probe pulse. In this manner, as was the case in Sec. III, the MCWP approach offers a very direct look into the timescale of the ionization dynamics associated with a given feature in the KER spectra. In Fig. 7, we also notice that the first jumps mainly occur at the

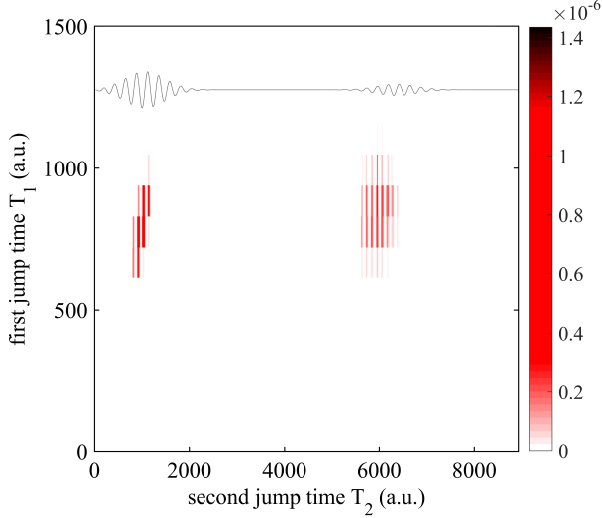


FIG. 7. Contributions from different trajectories to the four peaks (8.5 eV, 9.8 eV, 13 eV and 1.4 eV) in the KER spectra in Fig. 6(b) when the delay is 122 fs. The distributions in the small $T_2 \sim 1000$ range result in three high-energy peaks around 8.5 eV, 9.8 eV and 13 eV while the distributions in the large $T_2 \sim 6000$ range give the low-energy peak around 1.4 eV. The two pulses are also shown by the grey line in the top of the figure. To show the distributions clearly in a single figure, signals for $T_2 \sim 6000$ have been multiplied by a factor of 5000.

same time around 750 (18.3 fs) for the three high-energy peaks. The pump field is so strong that nearly all of the singly-ionized molecules would be further ionized in two laser cycles.

The evolution of the wave packet could be quite different when the wavelengths of the two pulses are different. In Fig. 8, the nuclear KER spectra of H_2 interacting with two pulses with different wavelengths are shown. The central wavelength of the pump pulse is 800 nm and that of the probe pulse is 6400 nm. They both contain three laser cycles. As the probe pulse is much longer, there are more structures and more yields in the KER spectra mainly induced by the probe pulse. Even when the delay reaches almost 70 fs, the overlap between the two pulses still plays a role in the final KER spectra, as is seen from the delay-dependence of the 10 eV channel. Moreover, there are more structures around the large kinetic energy channel at small delays as the effective duration of the pump pulse is becoming larger. Because of the complicated structures in the energy-decreasing branch (from 5 eV to 2 eV) in Fig. 8, the low-energy peaks in this case are not used to obtain the dissociative kinetic energy after the one-photon resonance.

The pronounced energy-decreasing branch in Fig. 8 is, however, useful for extracting information about CREI. The total KER spectra integrated over all delays in Figs. 5 and 8 are shown in Fig. 9, which shows a clear signature of the presence of the enhanced ionization. For

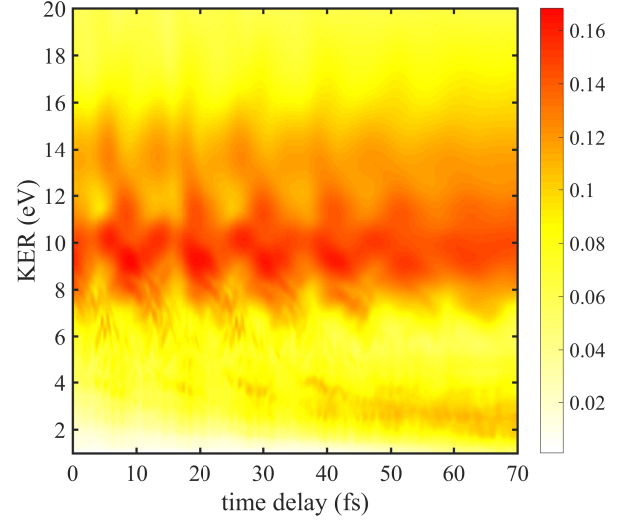


FIG. 8. Nuclear KER distributions as a function of time delay between the pump and probe pulses. The peak intensity of the pump (probe) pulse is 4×10^{14} W/cm² (6×10^{13} W/cm²). The pump (probe) wavelength is 800 nm (6400 nm). The duration of both pulses is 3 laser cycles. The data are plotted to the power of 0.2 in order to gain a larger visibility of the structures.

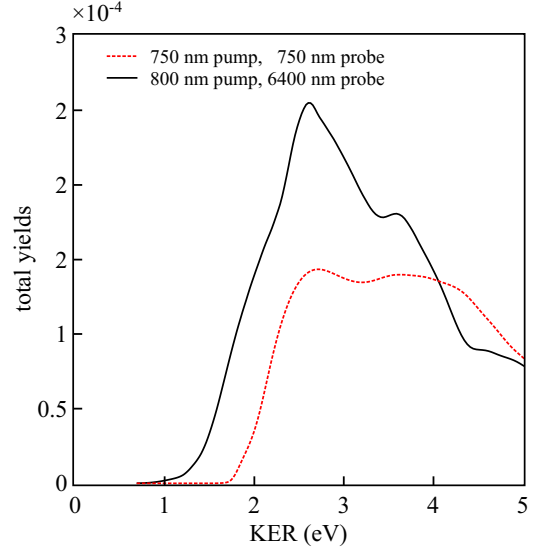


FIG. 9. Total KER spectra integrated over all delays and shown as a function of KER energy. The red dashed line is for Fig. 5 and the black solid line for Fig. 8, respectively.

both cases, the peaks around 3.6 eV mainly come from ionization at the CREI position of $R = 11$ after the one-photon resonance between the $2p\sigma_u$ and $1s\sigma_g$ curves in H_2^+ , while the energy-decreasing branch around 2.6 eV for delays larger than ~ 40 fs represents nuclear KER spectra resulting from ionization from $R > 11$. In theory, there should be peaks around 4.6 eV because of large ionization around the other CREI position at $R = 7$ after the one-photon resonance between the $2p\sigma_u$ and $1s\sigma_g$

curves in H_2^+ . However, they are not as clear as the peaks around 3.6 eV. A possible origin is that enhanced ionization at around $R = 7$ results in a broader energy peak than that at around $R = 11$ because of the fact that there is a larger relative change in the Coulomb repulsion energy at smaller internuclear distances than at larger internuclear distances for a given ΔR .

The above discussion shows how the wavelength, pulse duration as well as delay of the laser pulses determines the nuclear KER spectra. The dynamics of the nuclear wave packets can be extracted when these parameters are well chosen. The ionization induced by the probe pulse after the one-photon resonance resulting from the pump pulse largely contributes to the energy-decreasing branch of the KER spectra. This delay-dependent channel will be more pronounced if the duration or the intensity of the probe pulse is increased. Meanwhile, when increasing the duration of the laser pulses, CREI would also show up more clearly on the averaged spectra integrated over all delays.

V. SUMMARY AND CONCLUSION

We calculated the nuclear KER spectra of H_2 interacting with laser pulses with central wavelengths ranging from the near-IR regime to the mid-IR regime. With increasing wavelength, we observe a shift in the nuclear kinetic energy distribution towards lower energies. A detailed analysis of the peaks in the KER spectra was carried out. Some of the peaks are from ionization taking place at the one- or three-photon resonance between the $1s\sigma_g$ and $2p\sigma_u$ curves in the H_2^+ system. Others are from CREI after the one- and three-photon resonances, or from a combination of these processes. Both for the cases of a single laser pulse and for two time-delayed pulses, characteristic low-energy peaks were observed when the

duration or the delay of the pulses is large, e.g., for a single pulse with 21 laser cycles at 6400 nm and for two pump-probe pulses at 1600 nm with delay of 122 fs. The main physical origin of the low-energy peaks is ionization occurring at instants of field extrema when the nuclear wave packet has reached separations beyond the CREI position of $R = 11$. For the single pulse case, the low-energy peak is a result of ionization after dissociation via the one- and three-photon resonances between the $1s\sigma_g$ and $2p\sigma_u$ states. For the two pulse case, it mainly originates from ionization following dissociation via the one-photon resonance between the two states. In the pump-probe simulation, by integrating the KER spectra with all delays, the effect of CREI was shown in the KER spectra. We also showed how to extract the dissociative energies of the $2p\sigma_u$ curve in H_2^+ following excitation at the one- or three-photon resonances at 750 nm, 1600 nm and 6400 nm. Finally, we illustrated in a few selected cases how the MCWP approach allows a trajectory analysis helping with the identification of dominant breakup pathways including an assessment of typical durations between the ionization events forming the characteristic features in the KER spectra.

ACKNOWLEDGMENTS

We thank Lun Yue for help with numerical issues. This work was supported by the European Union Horizon 2020 research and innovation programme under the Marie Skłodowska-Curie grant agreement No. 641789 MEDEA (Molecular Electron Dynamics Investigated by Intense Fields and Attosecond Pulses), the European Research Council StG (Project No. 277767-TDMET), and the VKR center of excellence, QUSCOPE. The numerical results presented in this work were obtained at the Centre for Scientific Computing, Aarhus.

-
- [1] L. Zhu, V. Kleiman, X. Li, S. P. Lu, *et al.*, “Coherent laser control of the product distribution obtained in the photoexcitation of HI,” *Science* **270**, 77 (1995).
 - [2] A. H. Zewail, “Femtochemistry: Atomic-scale dynamics of the chemical bond,” *J. Phys. Chem. A* **104**, 5660–5694 (2000).
 - [3] I. V. Hertel and W. Radloff, “Ultrafast dynamics in isolated molecules and molecular clusters,” *Rep. Prog. Phys.* **69**, 1897 (2006).
 - [4] D. Rapp, P. Englander-Golden, and D. D. Briglia, “Cross sections for dissociative ionization of molecules by electron impact,” *J. Chem. Phys.* **42**, 4081–4085 (1965).
 - [5] K. Codling and L. J. Frasinski, “Dissociative ionization of small molecules in intense laser fields,” *J. Phys. B: At., Mol. Opt. Phys.* **26**, 783 (1993).
 - [6] S. Chelkowski, C. Foisy, and A. D. Bandrauk, “Electron-nuclear dynamics of multiphoton H_2^+ dissociative ionization in intense laser fields,” *Phys. Rev. A* **57**, 1176 (1998).
 - [7] J. H. Posthumus, “The dynamics of small molecules in intense laser fields,” *Rep. Prog. Phys.* **67**, 623 (2004).
 - [8] L. Yue and L. B. Madsen, “Dissociation and dissociative ionization of H_2^+ using the time-dependent surface flux method,” *Phys. Rev. A* **88**, 063420 (2013).
 - [9] T. Jahnke, A. Czasch, M. S. Schöffler, S. Schössler, A. Knapp, M. Kász, J. Titze, C. Wimmer, K. Kreidi, R. E. Grisenti, A. Staudte, O. Jagutzki, U. Hergenhahn, H. Schmidt-Böcking, and R. Dörner, “Experimental observation of interatomic Coulombic decay in neon dimers,” *Phys. Rev. Lett.* **93**, 163401 (2004).
 - [10] L. Strüder, S. Epp, D. Rolles, R. Hartmann, P. Holl, G. Lutz, H. Soltau, R. Eckart, C. Reich, K. Heinzinger, *et al.*, “Large-format, high-speed, X-ray pnCCDs combined with electron and ion imaging spectrometers in a multipurpose chamber for experiments at 4th generation light sources,” *Nucl. Instrum. Methods Phys. Res. A* **614**, 483–496 (2010).

- [11] U. Thumm, T. Niederhausen, and B. Feuerstein, “Time-series analysis of vibrational nuclear wave-packet dynamics in D_2^+ ,” *Phys. Rev. A* **77**, 063401 (2008).
- [12] A. D. Bandrauk and J. Ruel, “Charge-resonance-enhanced ionization of molecular ions in intense laser pulses: Geometric and orientation effects,” *Phys. Rev. A* **59**, 2153 (1999).
- [13] T. Zuo and A. D. Bandrauk, “Charge-resonance-enhanced ionization of diatomic molecular ions by intense lasers,” *Phys. Rev. A* **52**, R2511 (1995).
- [14] B. Yang, M. Saeed, L. F. DiMauro, A. Zavriyev, and P. H. Bucksbaum, “High-resolution multiphoton ionization and dissociation of H_2 and D_2 molecules in intense laser fields,” *Phys. Rev. A* **44**, R1458 (1991).
- [15] A. Apalategui and A. Saenz, “Multiphoton ionization of the hydrogen molecule H_2 ,” *J. Phys. B: At., Mol. Opt. Phys.* **35**, 1909 (2002).
- [16] S. Chelkowski, A. D. Bandrauk, A. Staudte, and P. B. Corkum, “Dynamic nuclear interference structures in the Coulomb explosion spectra of a hydrogen molecule in intense laser fields: Reexamination of molecular enhanced ionization,” *Phys. Rev. A* **76**, 013405 (2007).
- [17] J. Caillat, J. Zanghellini, M. Kitzler, O. Koch, W. Kreuzer, and A. Scrinzi, “Correlated multielectron systems in strong laser fields: A multiconfiguration time-dependent Hartree-Fock approach,” *Phys. Rev. A* **71**, 012712 (2005).
- [18] J. L. Sanz-Vicario, H. Bachau, and F. Martín, “Time-dependent theoretical description of molecular autoionization produced by femtosecond xuv laser pulses,” *Phys. Rev. A* **73**, 033410 (2006).
- [19] F. Calegari, D. Ayuso, A. Trabattini, L. Belshaw, S. De Camillis, S. Anumula, F. Frassetto, L. Poletto, A. Palacios, P. Decleva, J. B. Greenwood, F. Martín, and M. Nisoli, “Ultrafast electron dynamics in phenylalanine initiated by attosecond pulses,” *Science* **346**, 336–339 (2014).
- [20] J. Dalibard, Y. Castin, and K. Mølmer, “Wave-function approach to dissipative processes in quantum optics,” *Phys. Rev. Lett* **68**, 580 (1992).
- [21] H. A. Leth, L. B. Madsen, and K. Mølmer, “Monte Carlo wave packet theory of dissociative double ionization,” *Phys. Rev. Lett* **103**, 183601 (2009).
- [22] H. A. Leth, L. B. Madsen, and K. Mølmer, “Monte Carlo wave packet approach to dissociative multiple ionization in diatomic molecules,” *Phys. Rev. A* **81**, 053409 (2010).
- [23] H. A. Leth, L. B. Madsen, and K. Mølmer, “Dissociative double ionization of H_2 and D_2 : Comparison between experiment and monte Carlo wave packet calculations,” *Phys. Rev. A* **81**, 053410 (2010).
- [24] H. A. Leth and L. B. Madsen, “Dissociative multiple ionization of diatomic molecules by extreme-ultraviolet free-electron-laser pulses,” *Phys. Rev. A* **83**, 063415 (2011).
- [25] H.-P. Breuer, E.-M. Laine, J. Piilo, and B. Vacchini, “Colloquium: Non-Markovian dynamics in open quantum systems,” *Rev. Mod. Phys.* **88**, 021002 (2016).
- [26] M. Vafaee, H. Sabzyan, Z. Vafaee, and A. Katanforoush, “Detailed instantaneous ionization rate of H_2^+ in an intense laser field,” *Phys. Rev. A* **74**, 043416 (2006).
- [27] G. L. Yudin and M. Y. Ivanov, “Nonadiabatic tunnel ionization: Looking inside a laser cycle,” *Phys. Rev. A* **64**, 013409 (2001).
- [28] E. Goll, G. Wunner, and A. Saenz, “Formation of ground-state vibrational wave packets in intense ultra-short laser pulses,” *Phys. Rev. Lett.* **97**, 103003 (2006).
- [29] T. Ergler, B. Feuerstein, A. Rudenko, K. Zrost, C. D. Schröter, R. Moshhammer, and J. Ullrich, “Quantum-phase resolved mapping of ground-state vibrational D_2 wave packets via selective depletion in intense laser pulses,” *Phys. Rev. Lett.* **97**, 103004 (2006).
- [30] J. Förster, E. Plésiat, A. Magaña, and A. Saenz, “Imaging of the umbrella motion and tunneling in ammonia molecules by strong-field ionization,” *Phys. Rev. A* **94**, 043405 (2016).
- [31] B. Wolter, M. G. Pullen, M. Baudisch, M. Sclafani, M. Hemmer, A. Senftleben, C. D. Schröter, J. Ullrich, R. Moshhammer, and J. Biegert, “Strong-field physics with mid-IR fields,” *Phys. Rev. X* **5**, 021034 (2015).
- [32] C. I. Blaga, J. Xu, A. D. DiChiara, E. Sistrunk, K. Zhang, P. Agostini, T. A. Miller, L. F. DiMauro, and C. D. Lin, “Imaging ultrafast molecular dynamics with laser-induced electron diffraction,” *Nature* **483**, 194–197 (2012).
- [33] M. Meckel, D. Comtois, D. Zeidler, A. Staudte, D. Pavičić, H. C. Bandulet, H. Pépin, J. C. Kieffer, R. Dörner, D. M. Villeneuve, and P. B. Corkum, “Laser-induced electron tunneling and diffraction,” *Science* **320**, 1478–1482 (2008).
- [34] T. Popmintchev, M.-C. Chen, D. Popmintchev, P. Arpin, S. Brown, S. Ališauskas, G. Andriukaitis, T. Balčiūnas, O. D. Mücke, A. Pugzlys, A. Baltuška, B. Shim, S. E. Schrauth, A. Gaeta, C. Hernández-García, L. Plaja, A. Becker, A. Jaron-Becker, M. M. Murnane, and H. C. Kapteyn, “Bright coherent ultrahigh harmonics in the keV X-ray regime from mid-infrared femtosecond lasers,” *Science* **336**, 1287–1291 (2012).
- [35] X.-M. Tong, Z. X. Zhao, and C.-D. Lin, “Theory of molecular tunneling ionization,” *Phys. Rev. A* **66**, 033402 (2002).
- [36] X. Urbain, B. Fabre, E. M. Staicu-Casagrande, N. de Ruette, V. M. Andrianarijaona, J. Jureta, J. H. Posthumus, A. Saenz, E. Baldit, and C. Cornaggia, “Intense-laser-field ionization of molecular hydrogen in the tunneling regime and its effect on the vibrational excitation of H_2^+ ,” *Phys. Rev. Lett.* **92**, 163004 (2004).
- [37] O. I. Tolstikhin, T. Morishita, and L. B. Madsen, “Theory of tunneling ionization of molecules: Weak-field asymptotics including dipole effects,” *Phys. Rev. A* **84**, 053423 (2011).
- [38] J. Svensmark, O. I. Tolstikhin, and L. B. Madsen, “Theory of dissociative tunneling ionization,” *Phys. Rev. A* **93**, 053426 (2016).
- [39] P. J. Lindstrom and W. G. Mallard, “NIST chemistry webbook, NIST standard reference 69, june 2005,” National Institute of Standards and Technology, Gaithersburg MD, <http://webbook-.nist.gov> (2005).
- [40] H. A. Leth, *Dissociative ionization - a study using the Monte Carlo Wave Packet Approach*, PhD dissertation, Aarhus University, Department of Physics and Astronomy (2011).
- [41] M. Plummer and J. F. McCann, “Field-ionization rates of the hydrogen molecular ion,” *J. Phys. B: At., Mol. Opt. Phys.* **29**, 4625 (1996).
- [42] M. Feit, J. Fleck, and A. Steiger, “Solution of the schrödinger equation by a spectral method,” *Journal of Computational Physics* **47**, 412 – 433 (1982).
- [43] J. T. Lin and T. F. Jiang, “Photodissociation of H_2^+ in intense chirped laser fields,” *Phys. Rev. A* **63**, 013408

- (2000).
- [44] A. Staudte, D. Pavičić, S. Chelkowski, D. Zeidler, M. Meckel, H. Niikura, M. Schöffler, S. Schössler, B. Ulrich, P. P. Rajeev, T. Weber, T. Jahnke, D. M. Villeneuve, A. D. Bandrauk, C. L. Cocke, P. B. Corkum, and R. Dörner, “Attosecond strobing of two-surface population dynamics in dissociating H_2^+ ,” *Phys. Rev. Lett.* **98**, 073003 (2007).
 - [45] H. Niikura, D. M. Villeneuve, and P. B. Corkum, “Controlling vibrational wave packets with intense, few-cycle laser pulses,” *Phys. Rev. A* **73**, 021402(R) (2006).
 - [46] I. A. Bocharova, H. Mashiko, M. Magrakvelidze, D. Ray, P. Ranitovic, C. L. Cocke, and I. V. Litvinyuk, “Direct Coulomb-explosion imaging of coherent nuclear dynamics induced by few-cycle laser pulses in light and heavy hydrogen,” *Phys. Rev. A* **77**, 053407 (2008).
 - [47] A. S. Alnaser, X. M. Tong, T. Osipov, S. Voss, C. M. Maharjan, P. Ranitovic, B. Ulrich, B. Shan, Z. Chang, C. D. Lin, and C. L. Cocke, “Routes to control of H_2 Coulomb explosion in few-cycle laser pulses,” *Phys. Rev. Lett.* **93**, 183202 (2004).
 - [48] H. Xu, F. He, D. Kielpinski, R. T. Sang, and I. V. Litvinyuk, “Experimental observation of the elusive double-peak structure in R-dependent strong-field ionization rate of H_2^+ ,” *Sci. Rep.* **5**, 13527 (2015).